Structural connectome topology relates to regional BOLD signal dynamics in the mouse brain

Sarab S. Sethi*,[1, a)] Valerio Zerbi*,[2] Nicole Wenderoth,[2] Alex Fornito,[3] and Ben D. Fulcher[3, b)]
[1)] *Department of Mathematics, Imperial College London, UK*
[2)] *Neural Control of Movement Lab, Department of Health Sciences and Technology, ETH Zurich, Switzerland*
[3)] *Brain and Mental Health Laboratory, Monash Institute of Cognitive and Clinical Neurosciences, School of Psychological Sciences and Monash Biomedical Imaging, Monash University, Melbourne, Australia*

(Dated: 5 November 2016)

Brain dynamics unfold on a network determined by the pattern of axonal connections linking pairs of neuronal populations; the so-called connectome. Prior work has indicated that structural brain connectivity constrains pairwise correlations in brain dynamics (also called functional connectivity), but it is not known whether brain network structure is related to the intrinsic dynamics of individual brain regions. In this study, we investigate the relationship between a brain region's inter-regional axonal connectivity and its dynamics using a weighted, directed mesoscale mouse connectome from the Allen Mouse Brain Connectivity Atlas and resting state functional MRI (rs-fMRI) time-series data measured in 184 brain regions in eighteen anesthetized mice. Three properties of a brain region's structural network connectivity were measured–degree, betweenness, and clustering coefficient–from weighted and unweighted, and directed and undirected versions of the connectome. We then characterised the univariate rs-fMRI dynamics at each brain region by computing 6 930 time-series properties using recently developed highly comparative time-series analysis software, *hctsa*. We found that strong and robust relationships between the inter-regional axonal connectivity of a brain region and its intrinsic fMRI dynamics were mediated by the weighted in-degree, the total weight of incoming connections to a brain region, emphasizing the importance of measuring weight and directionality of network connections. Brain regions with increased weighted in-degree exhibit rs-fMRI dynamics with reduced variance (correlation to standard deviation, $\rho = -0.62$), and slower correlation timescales (correlation to relative high frequency power, $f \geq 0.375\,\text{Hz}$, $\rho = -0.58$), relationships that were reproduced in each of the eighteen individual mice that underwent rs-fMRI. Our results indicate that the topology of inter-regional axonal connections of the mouse brain is closely related to the intrinsic, spontaneous dynamics occurring within a region and that variations in the aggregate strength of incoming projections to a region are associated with both the variability and timescales of that region's activity fluctuations.

Nervous systems are complex networks with a topology governed by the pattern of axonal connections linking distinct neural elements. Accordingly, highly connected and topologically central neural elements are thought to play an important role in meditating the flow of information across different parts of the system. However, it is unclear how the intrinsic dynamics of a given neuronal population relates to the pattern of connections that population shares with other network nodes. In this work, we show that there is a strong and robust correlation between the structural connectivity properties of a brain region and its blood-oxygenation-level-dependent (BOLD) signal dynamics, as measured with resting-state fMRI in the mouse. The relationship is driven by the total weight of incoming connections to a brain region, with increased incoming connectivity associated with a tighter distribution of BOLD values (decrease in the standard deviation), and longer dynamical timescales (decrease in relative power in frequencies $f \geq 0.375\,\text{Hz}$). Our findings indicate that the weights and directions of structural connections convey vital information about neural activity, and that the aggregate strength of incoming projections to a brain region is intimately related to its BOLD signal dynamics.

I. INTRODUCTION

The principle that structure constrains function is ubiquitous in biology. For example, the molecular structure of a protein determines the species with which it can interact. Similarly, the evolution of opposable thumbs in some primate species enabled high-precision motor control. Brains are no exception, with neuronal dynamics unfolding on an intricate and topologically complex network of axonal connections; a network that is commonly referred to as a connectome[1]. In a graph representation of this network, nodes comprise functionally homogeneous or anatomically localized neurons or populations

[a)] s.sethi16@imperial.ac.uk
[b)] ben.fulcher@monash.edu

of neurons (depending on the scale of measurement), and axonal connections between these neural elements are represented as edges connecting pairs of nodes.

The network representation of the brain has provided a convenient framework for understanding the relationship between connectome structure and brain dynamics. This relationship has typically been examined at the level of inter-regional structural connectivity and inter-regional coupling of brain dynamics, or functional connectivity. Correlations between structural and functional connectivity have been demonstrated using a range of approaches and datasets[2–8], with computational modelling playing a key role. Computational models of brain networks typically simulate dynamical systems (which define the dynamics of each brain region) coupled via a network topology determined by the structural connectome[3,5,8–11]. These models range in complexity from nonlinear biophysically-based models[9,12–14], linear models[15–17], and Kuramoto models[18–20]. Some models can predict empirical measurements of functional connectivity in human with model predictions correlating with empirical data in the range $0.4 < r < 0.6$[21], and can be optimized up to $r = 0.75$[22]. These results are impressive given the known limitations of diffusion MRI in reconstructing anatomical brain connections[6,23]. Interestingly, the prediction of empirical functional connectivity from model-based estimates is maximal for parameter regimes in which the model operates close to a critical point of a bifurcation, i.e., near the edge of an instability[21,22,24,25]. The success of this broad array of dynamical systems models, as well as simplified network spreading models[23,26,27], in reproducing the correlation structure of inter-regional brain dynamics suggests that the structural connectome plays a powerful role in constraining brain dynamics.

While there is a growing evidence base linking the structural topology of a brain network to the inter-regional coupling of functional connectivity, less is known about how connectome structure relates to the intrinsic dynamics of an individual brain region. Understanding this relationship would provide insight into how patterns of neuronal activity within a given brain region may support its specialized function. Indeed, in addition to inter-regional variation in microstructural properties and gene transcription[28,29], it has long been thought that the functional specialization of a given brain region is in large part determined by its unique profile of axonal inputs and outputs – its so-called connectional fingerprint[30]. Moreover, recent work using magnetoencephalography (MEG) has suggested that the dynamics of individual brain regions (captured using power spectral estimates through time) are sufficiently distinctive to be predicted across individuals[31]. Other evidence indicates that brain dynamics are governed by a hierarchy of intrinsic timescales across regions, from slowly-varying prefrontal areas high in the anatomical hierarchy[32] (the slower timescales allowing integration of diverse inputs), to the relatively rapid dynamics of sensory regions low in the hierarchy (that respond more quickly to incoming stimuli)[20,33–37]. This hierarchical organization of timescales across the brain may facilitate processing of the diverse timescales of stimuli the world around us, as well as the timescales required to make useful predictions about those stimuli. Computational modeling has begun to shed light on the role of connectivity in shaping this inter-regional heterogeneity in characteristic timescales[14], including the emergence of slow oscillations in densely connected, high-degree brain network hubs in identical, connectome-coupled neural mass models[13]. Thus, although preliminary modeling work has suggested that the connectome may play a role in shaping dynamical heterogeneity across the brain, empirical data has been lacking to allow a thorough characterization of the relationship between connectivity and dynamics at the level of individual brain regions.

Compared to measures of pairwise correlation between time series that yield estimates of functional connectivity, a key challenge of analyzing the univariate dynamics of individual brain regions is the vast array of properties that can be estimated for a give time series recording of neuronal activity. Previous analysis of univariate fMRI dynamics has focused on properties of the power spectrum, such as the total power in particular frequency bands[51]. However, quite apart from properties of the power spectrum, thousands of alternative time-series analysis methods exist that might contain useful information, such as those developed for applications in statistics, electrical engineering, economics, statistical physics, dynamical systems, and biomedicine[38]. Here we leverage this vast interdisciplinary library of time-series analysis methods to characterize the fluctuations of spontaneous regional activity using resting-state fMRI (rs-fMRI), using a recently developed highly comparative analysis framework that extracts over 7 700 properties from univariate time series[38,39]. In this way, we computed thousands of properties of the intrinsic rs-fMRI dynamics in each brain region using data from 18 anesthetized mice. We also characterized the network connectivity properties of each brain region using a mesoscale mouse connectome inferred from viral tract-tracing experiments[40]. Comparing the two measurements, we demonstrate robust correlations between a brain region's structural connectivity and its dynamics, with the strongest relationship found between weighted in-degree and (i) decreased standard deviation of rs-fMRI dynamics, and (ii) decreased relative spectral power in frequencies $f \geq 0.375$ Hz. Our results are consistent with the idea that the structural connectome constrains regional rs-fMRI dynamics and underline the importance of measuring directed and weighted information for probing the structure-function relationship.

II. DATA AND METHODS

Our approach for relating structural connectivity to regional rs-fMRI dynamics is shown schematically in Fig. 1. It involves: (i) extracting topological measures from each node in the network from the structural connectome; (ii) extracting dynamical properties from the fMRI time series measured in each brain region; and (iii) correlating each network property to each dynamical feature. In this section, we will first summarize the structural connectivity and functional MRI data used in this study, and then go on to detail the methods used for each of the above steps.

A. Structural connectivity data

The mesoscale structural connectome of the mouse brain was derived from 469 viral microinjection experiments in C57BL/6J male mice at age P56, obtained from the Allen Mouse Brain Connectivity Atlas (AMBCA)[40]. These data were summarized in the form of a weighted, directed connectivity matrix containing 213 brain regions from the Allen Reference Atlas ontology[41] using a regression model[40]. The model yields a normalized connection strength (or weight) and a p-value for each edge in the connectome, quantifying the estimated confidence that the connection is spurious. Here we analyze the 213×213 connectivity matrix corresponding to ipsilateral connectivity between regions in the right hemisphere of the mouse brain, including only edges with $p < 0.05$ (and excluding self-connections), resulting in a link density of 6.9%. We focus on results using this full ipsilateral connectome, but also tested the robustness of the results when including contralateral connectivity. From contralateral connectivity data from the right hemisphere $\rightarrow$ left hemispheres[40], we extrapolated a complete connectome under the assumption of hemispheric symmetry (as Rubinov et al. [65]), in which connections from the left to the right hemisphere match those from right to left hemisphere exactly, and ipsilateral connectivity within the left hemisphere mirrors that within the right hemisphere.

B. Functional MRI data

a. Mice All experiments were performed in accordance to the Swiss federal guidelines for the use of animals in research, and under a license from the Zürich Cantonal veterinary office. Animals were caged in standard housing, with food and water ad libitum, and 12 h day and night cycle.

b. Magnetic resonance imaging Eighteen C57BL/6J mice (age P57 $\pm$7) were used for this experiment. During the MRI session, the levels of anesthesia and mouse physiological parameters were monitored following an established protocol to obtain a reliable measurement of functional connectivity[42]. Briefly, anesthesia was induced with 4% isoflurane and the animals were endotrachally intubated and the tail vein cannulated. Mice were positioned on a MRI-compatible cradle, and artificially ventilated at 80 breaths per minute, 1:4 O_2 to air ratio, and 1.8 ml/h flow (CWE, Ardmore, USA). A bolus injection of medetomidine 0.05 mg/kg and pancuronium bromide 0.2 mg/kg was administered, and isoflurane was reduced to 1.5%. After 5 min, an infusion of medetomidine 0.1 mg/kg/h and pancuronium bromide 0.4 mg/kg/h was administered, and isoflurane was further reduced to 0.5%. The animal temperature was monitored using a rectal thermometer probe, and maintained at 36.5 ± 0.5°C during the measurements. The preparation of the animals did not exceed 20 minutes. After the scans, mice were kept in a temperature-controlled chamber under mechanical ventilation until they were able to breath spontaneously. All animals fully recovered after 30 minutes from the end of the experiment and transferred back to their own cages. Data acquisition was performed on a Pharmascan 7.0 small animal MR system operating at 300 MHz (Bruker BioSpin MRI, Ettlingen, Germany). A high SNR receive-only cryogenic coil (Bruker BioSpin AG, Fällanden, Switzerland) is used in combination with a linearly polarized room temperature volume resonator for transmission. Images were acquired using Paravision 6 software. After standard adjustments, shim gradients were optimized using mapshim protocol, with an ellipsoid reference volume covering the whole brain. Resting-state fMRI (rs-fMRI) was performed with gradient-echo echo planar images (GE-EPI) that were acquired with repetition time TR = 1000 ms, echo time TE = 15 ms, flip angle = 60°, matrix size = 90×50, in-plane resolution = $0.22 \times 0.2\,\mathrm{mm}^2$, number of slice = 20, slice thickness ST = 0.4 mm, slice gap SG = 0.1 mm, 2000 volumes, for a total scan time of 38 min. Anatomical T1-weighted images were acquired with same orientation as the GE-EPI using a FLASH-T1 sequence (TE = 3.51 ms, TR = 522 ms, flip angle = 30°, in-plane resolution = $0.05 \times 0.02\,\mathrm{mm}^2$, ST = 0.5 mm).

c. Data preprocessing Resting state fMRI datasets were preprocessed using an existing pipeline for removal of unwanted confounds from the time-series[42], with modifications (Fig. S2). Briefly, each rs-fMRI dataset was fed into MELODIC (Multivariate Exploratory Linear Optimized Decomposition of Independent Components[43]) to perform within-subject spatial-ICA with a fixed dimensionality estimation (number of components set to 100). This included high-pass filtering (> 0.01 Hz), correction for head motion using MCFLIRT[44] and in-plane smoothing with a 0.3×0.3 mm kernel. We applied FSL-FIX with a study-specific classifier obtained from an independent dataset of 15 mice and used a 'conservative' removal of the variance of the artefactual components (for more details, see[45]). Thereafter, FIX-cleaned datasets were co-registered into the skull-stripped T1-weighted images and normalized into AMBMC template (`www.imaging.org.au/AMBMC`) using ANTs v2.1 (`picsl.upenn.edu/ANTS`).

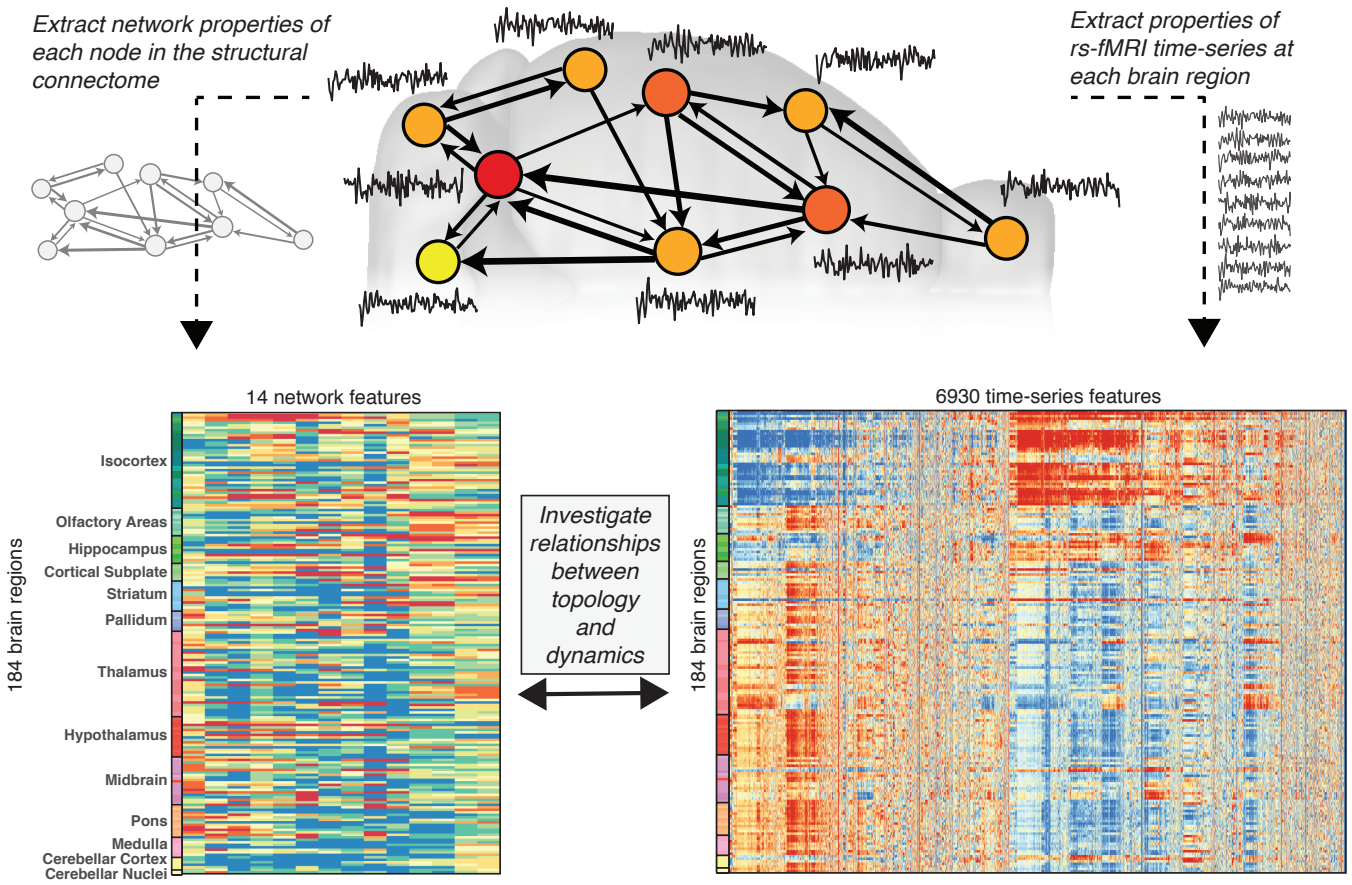

FIG. 1. **Relating inter-regional connection topological to intrinsic regional dynamics.** A schematic illustration of the mouse structural connectome (top), in which the brain is represented as a set of nodes (macroscopic brain regions), and axonal connections between regions are represented as directed edges (shown as arrows) with a weight reflecting the connection strength (shown as line width). Different properties can then be computed for each brain region according to their network connectivity properties; the example plotted here is number of connections projecting out of a brain region, also known as 'out degree' (shown using color from low, yellow, to high, red). In addition, spotaneous blood-oxygenation-level-dependent (BOLD) dynamics were measured for each brain region using fMRI (shown as time series). Here we compute 14 different network properties for 184 brain regions from the mesoscale structural connectome (lower, left) and, independently, compute 6 930 time-series properties of the univariate fMRI dynamics measured in the same set of brain regions (lower, right). In these lower plots, each row represents a brain region (labeled by broad anatomical divisions of the mouse brain[40,41]), and each column represents a property computed for all brain regions, derived from either the structural connectome (lower, left), or the BOLD time-series dynamics (lower, right). Color encodes the output of each property, from low values (blue) to high values (red). The aim of this study was to determine whether the fMRI dynamics of a brain region can be predicted from its structural connectivity properties by searching for correlations between structural network features and dynamical features across the brain.

Time series were extracted from 370 anatomical regions using the Allen Reference Atlas ontology[41], as in Oh et al.[40]. Only regions that were fully covered by the field of view used for fMRI acquisition were included in the analysis. These regions were then matched to the Allen Mouse Connectivity Atlas, above, yielding a total of 184 matching brain regions for each hemisphere. Here we focus on regions in the right hemisphere, for which full structural connectivity data is available (see above). Thus, the final rs-fMRI dataset consisted of 2 000-sample time series in 184 brain regions for 18 mice, a total of 3 312 time series.

C. Topological node measures

In order to characterize the connectivity of each brain region, we used the 213-node, ipsilateral connectome described above to calculate node properties (note that, due to data availability, only 184 of these brain regions were able to be matched to rs-fMRI dynamics). We focused on three key properties: (i) degree; (ii) betweenness centrality; and (iii) clustering coefficient (described in detail below). These measures were chosen as they encapsulate conceptually different network properties, and are commonly used in the literature. To assess the role of

edge weights and edge directionality, we computed these three node properties for four different types of networks, where possible: (i) the original directed, weighted connectome (see above); (ii) a directed, unweighted connectome; (iii) an undirected, weighted connectome; and (iv) an undirected, unweighted connectome. To transform weighted networks to unweighted networks, we assigned a unit weight to all edges with non-zero weight, and to transform directed networks to undirected networks, we assigned edge weights as the sum of the edge weights in and out of each node in the original network. The measures are described in turn below.

d. Degree For a directed, unweighted network, the in-degree, $k_{\text{in}}(i)$, of node i is defined as the number of incoming edges, and the out-degree, $k_{\text{out}}(i)$, is defined as the number of outgoing edges. On undirected networks, the lack of directional information means that only the total degree, $k(i)$, can be computed, which is defined as the total number of connections involving node i. On weighted networks, the concept of degree can be extended to incorporate edge weights, where the weighted counterpart of node degree (also known as 'node strength') sums the weights on edges rather than counting them. For example, the weighted in-degree, $k_{\text{in}}^{w}(i)$ is the sum of the edge weights on the incoming edges to node i.

e. Betweenness centrality The betweenness centrality of a node, i, is given by

$$b(i) = \frac{1}{(n-1)(n-2)} \sum_{\substack{h,j \in N \\ h \neq j, h \neq i, j \neq i}} \frac{\rho_{hj}(i)}{\rho_{hj}}, \qquad (1)$$

where N is the set of all nodes in the network, n is the number of nodes, ρ_{hj} is the total number of shortest paths between nodes h and j, and $\rho_{hj}(i)$ is the number of those paths that pass through node i[46]. For a binary network, all edges have the same weight, and the shortest path between nodes h and j is the path that minimises the number of edges that must be traversed. In a weighted network, a distance metric is defined for each link as the inverse of the edge weight. On a directed network, the shortest path must follow the direction of the edges. Assuming shortest path information transfer, a node with high betweenness centrality is more likely to be involved in mediating signal traffic across the network, with b thus providing an index of node 'centrality'.

f. Clustering coefficient The clustering coefficient of a node, i, in an unweighted undirected network is given by

$$C(i) = \frac{2e(i)}{k(i)(k(i)-1)}, \qquad (2)$$

where $k(i)$ is the degree of node i and $e(i)$ is the number of connected pairs between all neighbours of node i[47]. The clustering coefficient of node i is equivalent to the link density of its neighbors, such that $C(i) = 1$ indicates that node i and its neighbours form a clique, i.e., a fully connected subgraph. On an unweighted, directed network, the clustering coefficient of node i is defined similarly as $C^{\rightarrow}(i) = e(i)/[k(i)(k(i)-1)]$. The equation is modified because there are twice as many possible links between nodes in a directed network as compared with in an undirected network. Weighted generalisations of the clustering coefficient aim to capture the average intensity with which the neighbours of a node are connected. For weighted undirected networks, we use the measure given by Onnela et al.[48], and for weighted directed networks we use the measure in Fagiolo[49].

Applying the above three measures to the four types of networks (where possible), we computed a total of fourteen topological measures for each node: in-degree, out-degree, betweenness and clustering coefficient on the directed weighted and unweighted networks, and degree, betweenness and clustering coefficient on the undirected weighted and unweighted networks. All measures were calculated using implementations provided in the Brain Connectivity Toolbox[50] (functions used are listed in Supplementary Table S1).

D. Feature-based representation of rs-fMRI time series

Having quantified different aspects of nodal network connectivity, we next aimed to quantify the rs-fMRI dynamics at each node. Typically, blood-oxygenation-level-dependent (BOLD) time series are characterized using properties, or *features*, like the amplitude of low-frequency (0.01-0.08 Hz) fluctuation, ALFF[51]. Although spectral properties like ALFF are a natural representation of stationary oscillatory signals (as is often appoximately the case in brain recordings), there are thousands of alternative time-series analysis methods that could be used to meaningfully quantify regional rs-fMRI dynamics. These methods include measures of autocorrelation, temporal entropy, distributional spread, outlier properties, stationarity, wavelet transforms, time-delay embeddings, and fits to various time-series models. Rather than manually selecting a small number of such features, here we aimed to determine the most informative time-series features for understanding structural connectivity properties in a purely data-driven way. To achieve this, we used the highly comparative time-series analysis software package, *hctsa* (v0.91, `github.com/benfulcher/hctsa`)[38,39,52] to extract a total of 7 754 informative features from each of the 3 312 BOLD time series in our dataset (cf. Fig. 1, lower right). Each of the 7 754 features corresponds to a single interpretable measure of a regional BOLD time series, that could then be related to structural network connectivity properties.

Features that did not return a real number for all 3 312 time series in the full dataset (e.g., methods that relied on fitting positive-only distributions to our real-valued rs-fMRI data or methods attempting to fit complicated nonlinear time-series models that were not appropriate for these data), or features that returned an approximately constant value across the dataset (standard devi-

ation $< 2 \times 10^{-15}$) were removed from the set of features prior to analysis, resulting in a reduced set of 6 930 well-behaved time-series features. The results of the massive feature extraction facilitated by *hctsa*, could thus be represented as a 184 (brain region) $\times$ 6 930 (time-series feature) matrix that summarizes a diverse array of BOLD time-series properties in each mesoscale brain region for each mouse. To obtain a group-level understanding of the dynamics, we averaged features across all 18 mice for each brain region, yielding an averaged 184 $\times$ 6 930 (brain region) $\times$ (time-series feature) matrix, which is plotted in Fig. 1 (lower, right). This ensured that the features capture overall characteristics of the BOLD signal at each brain region, averaging over inter-individual and inter-scan variability. In addition to obtaining group-averaged results, we also investigated robustness at the level of each individual mouse, in which case the individual-specific time-series feature matrices (18 different 184 $\times$ 6 930 matrices) were analyzed separately.

E. Connecting topology to dynamics

Having characterized each brain region in terms of its (i) nodal properties in the structural connectome, and (ii) BOLD dynamics, we next sought to find correlations between these two independent measurements. For each of the fourteen connectivity properties, we computed Spearman's rank correlation coefficient, ρ, and an associated p-value, for each of the 6 930 time-series features (across all 184 brain regions). We used Spearman's rank correlations throughout this work, allowing statistical comparison between the frequently non-normally distributed nodal properties (especially those derived from weighted connectomes) and time-series properties. The family wise error rate was controlled using the Holm-Bonferroni method[53], correcting across 6 930 independent tests at a significance level of $p_{\text{corrected}} < 0.05$. Note that we are correcting for 6 930 independent tests even though there are approximately 200 linearly independent time-series behaviors in our feature set due to the existence of sets of highly correlated time-series features (cf. Fulcher et al.[38]). Our results thus constitute a conservative estimate of the number of time-series features that are significantly related to each topological quantity, minimising the false positive rate (type I error) at the cost of artificially inflating the false negative rate (type II error).

III. RESULTS

Our results are presented in three parts. First, we compare nodal network properties derived from weighted/unweighted and directed/undirected connectomes, in their correlations to the properties of rs-fMRI dynamics across the brain. We show that robust correlations between structural network topology and dynamics exist at the level of individual brain regions, and that the relationship is driven by the weighted in-degree, k^w_{in}, demonstrating the importance of measuring edge weights and directionality for addressing our hypothesis. We then characterize the types of rs-fMRI time-series properties that are most strongly correlated to weighted in-degree, k^w_{in}. Lastly, we demonstrate that the correlations hold not only on the group level, but also at the level of individual mice.

A. Comparison of topological measures and network types

We first address the question of whether the extrinsic axonal connectivity of a brain region is related to its intrinsic rs-fMRI dynamics. We computed fourteen structural network measures: degree, betweenness, and clustering coefficient, computed from weighted and unweighted, and directed and undirected versions of the connectome, from each of 184 brain regions, and indepedently computed 6 930 time-series features derived from the rs-fMRI BOLD signal in the same set of brain regions. We evaluated the relationship of each structural network property to the rs-fMRI time-series properties using Spearman correlations, as depicted in Fig. 1 (see Methods for details).

Results summarizing the relationship between each structural network property and rs-fMRI dynamics are shown in Fig. 2(a). For each network measure, the figure shows: (i) the magnitude of the strongest Spearman correlation, $|\rho|$, across all 6 930 rs-fMRI time-series features (using color); and (ii) the number of time-series features that exhibit a significant correlation, Holm-Bonferroni $p_{\text{corrected}} < 0.05$ (using text annotations). Note that since in- and out-degree cannot be computed from undirected networks; rectangular boxes in the upper right hand quarter of Fig. 2(a) indicate results for degree, k (unweighted) and k^w (weighted).

Although we summarize the results using the maximum correlation, $|\rho|$ in Fig. 2(a), the comparison of each network property to 6 930 rs-fMRI time series properties is best represented as a distribution of correlations, such as that shown in Fig. 2(b) for weighted in-degree, k_{in}. Figure 2(b) indicates the thresholds for Holm-Bonferroni $p_{\text{corrected}} < 0.05$ (vertical blue lines), revealing a large number of rs-fMRI properties that correlate strongly and significantly with k^w_{in} across 184 mouse brain regions, with correlations, $|\rho|$, reaching up to 0.68. Similar distributions for all node measures are in Supplementary Fig. S4.

Edge weights vary over many orders of magnitude, from a normalized connection density of 2.91×10^{-4} for the weakest connection to 20.4 for the strongest connection (cf. Fig. S1). Node-level structural network properties are therefore highly sensitive to the incorporation of edge weights. Overwhelmingly, network properties derived from the weighted connectome are more strongly correlated to properties of rs-fMRI time series than those

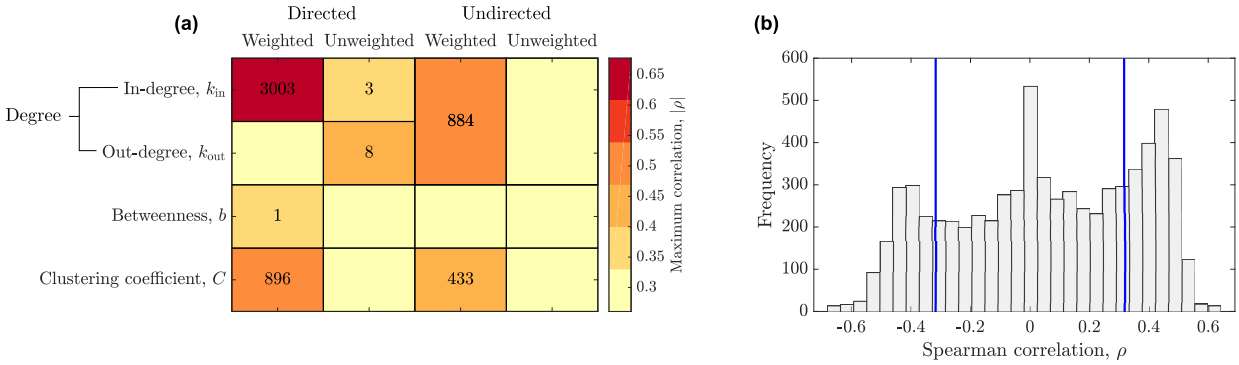

FIG. 2. **Regional structural network connectivity properties correlate with properties of regional rs-fMRI dynamics. (a)** We compare the degree, k, betweenness, b, and clustering coefficient, C, for (i) directed and undirected, and (ii) weighted and unweighted structural brain networks. For each nodal network property, we computed the magnitude of the strongest Spearman correlation, $|\rho|$, across 6 930 time-series features of the rs-fMRI signal (shown using color), and the number of time-series features that are significantly correlated with that property (Holm-Bonferonni $p_{\text{corrected}} < 0.05$) across all 184 brain regions (annotated with numbers; missing numbers indicate zero significant features). We see that taking edge weights into account is crucial for obtaining a strong correlation between regional connectivity and dynamics, and that edge directionality is also important. **(b)** The distribution of Spearman correlations, ρ, of weighted in-degree, k_{in}^{w} with 6 930 time-series features of rs-fMRI (correlations computed across 184 brain regions). Vertical blue lines indicate Holm-Bonferonni significance thresholds at $p_{\text{corrected}} < 0.05$.

computed from the unweighted connectome. For example, for in-degree and clustering coefficient, strong and significant correlations with time-series features present in the weighted networks are strongly diminished (or vanish) when computed from unweighted connectomes. As well as edge weights, our results also point to an important role of edge directionality for uncovering the relationship between structural connectivity and dynamics. All node measures, from both weighted and unweighted connectomes, showed stronger correlations to rs-fMRI dynamics when edge directionality was taken into account.

Of the three nodal structural connectome properties analyzed here, the immediate measure of connectivity, degree, k, showed the strongest correlations to regional rs-fMRI dynamics. While a moderate correlation was found using the undirected weighted degree, k^{w} (up to $|\rho| = 0.49$), when distinguishing incoming and outgoing connectivity pathways, our results reveal a strong asymmetry, with weighted in-degree, k_{in}^{w} showing the strongest correlations to rs-fMRI dynamics of all topological properties (up to $|\rho| = 0.68$), while weighted out-degree, k_{out}^{w} showed no significant correlations. This demonstrates the relative importance of incoming structural connectivity for understanding regional BOLD dynamics. In addition to degree, we found significant, but weaker correlations between clustering coefficient and properties of the rs-fMRI dynamics. In the directed network, $C^{\rightarrow,w}$ significantly correlated with 896 time-series features (up to $|\rho| = 0.49$), while C^{w} computed from the undirected network was significantly correlated with 433 time-series features ($p_{\text{corrected}} < 0.05$). Reiterating the importance of edge weights in uncovering relationships between structural connectivity and BOLD dynamics, unweighted versions of the clustering coefficient, $C^{\rightarrow}$ and C, exhibited no significant correlations to time-series features ($p_{\text{corrected}} < 0.05$). Betweenness centrality was the least informative nodal connectivity property for understanding rs-fMRI dynamics. Only one of the 6 930 time-series features correlated significantly with weighted directed betweenness, $b^{\rightarrow,w}$, ($|\rho| = 0.36$) and there were no significant correlations for $b^{\rightarrow}$, b^{w}, or b.

To understand the relationship between network connectivity measures and dynamics in more detail, we analyzed interrelationships between the structural network properties. Figure 3 shows inter-relationships between network properties derived from different connectomes as a pairwise Spearman correlation plot, where correlations were computed across all 184 brain regions. The plot show that the fourteen network connectivity measures computed here are not independent, in some cases forming clusters of inter-correlated nodal measures.

Figure 3 shows that many unweighted structural network properties are highly inter-correlated. For example, correlations between unweighted network properties: b, $b^{\rightarrow}$, k, C and $C^{\rightarrow}$ are all higher correlated to each other, $|\rho| \geq 0.72$ (with C and $C^{\rightarrow}$ negatively correlated to b, $b^{\rightarrow}$, and k), forming a cluster in the centre of Fig. 3. By contrast, the weighted counterparts of these measures: b^{w}, $b^{\rightarrow,w}$, k^{w}, C^{w} and $C^{\rightarrow,w}$, were less strongly correlated to each other. A similar result is seen for b and C, which are highly correlated across brain regions ($\rho = -0.92$), whereas the weighted versions b^{w} and C^{w} are much more weakly correlated ($\rho = 0.11$). The wide distribution of edge weights, across many orders of magnitude (cf. Fig. S1), allows the weighted network properties to capture distinct types of information than their unweighted counterparts that treat all edges are equivalent.

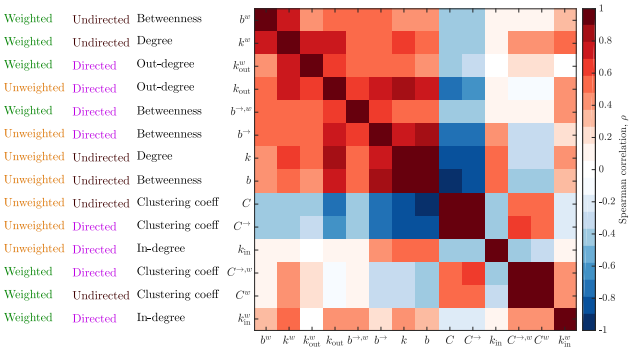

FIG. 3. **Correlation structure of topological descriptors of inter-regional structural connectivity.** Each column (and, equivalently, row) represents one of the fourteen different network properties, and each element of the plot represents a Spearman correlation between the corresponding pair of node measures, computed across 184 brain regions. Rows (and columns) have been reordered by hierarchical clustering, using an absolute correlation-based distance metric, $1 - |\rho|$, to place similar node properties close to each other. Nodal network properties are named according to the network type from which they were derived: directed or undirected, weighted or unweighted.

The topological property with the strongest correlation to rs-fMRI dynamics is the weighted in-degree, k_{in}^w, with $|\rho|$ reaching up to 0.68 ($p_{\text{corrected}} < 7.0 \times 10^{-21}$), consistent with a simple model of directed influence in which the BOLD signal fluctuations of a node are most strongly influenced by other brain regions projecting to it. Interestingly, we find that other structural connectivity properties that are correlated to rs-fMRI dynamics tend to be correlated with weighted in-degree, k_{in}^w. For example, weighted degree computed from the undirected network, k^w, is correlated with weighted in-degree, k_{in}^w ($\rho = 0.56$) and is also correlated to properties of the rs-fMRI dynamics (exhibiting significant correlations to 884 features). The weighted clustering coefficients, C^w and $C^{\rightarrow,w}$, were correlated with weighted in-degree, k_{in}^w ($\rho = 0.38$ for both), and were significantly correlated with rs-fMRI dynamics, whereas the unweighted clustering coefficients, C and $C^{\rightarrow}$ were less strongly correlated with k_{in}^w ($\rho = -0.21$, $|\rho| = -0.18$ respectively) and showed no significant correlations with any time series features, see Fig. 2(a). We tested the idea that k_{in}^w is mediating the relationship between structural connectivity and rs-fMRI dynamics, focusing on the three features other than k_{in}^w that exhibit strong and statistically significant correlations to rs-fMRI dynamics: C^w, $C^{\rightarrow,w}$, and k^w. To do this, we computed partial correlations to all 6 930 rs-fMRI time-series features, controlling for the effect of weighted in-degree, k_{in}^w. The number of time-series features that were significantly related to these measures dropped dramatically ($p_{\text{corrected}} < 0.05$): C^w ($433 \rightarrow 1$), $C^{\rightarrow,w}$ ($896 \rightarrow 1$), and k^w ($884 \rightarrow 3$). Thus, the relationship between C^w, $C^{\rightarrow,w}$, and k^w and rs-fMRI dynamics is mainly due to their correlation with k_{in}^w, indicating that they are not capturing interesting new information about rs-fMRI dynamics beyond what is captured by k_{in}^w. We conclude that the relationship between network properties and rs-fMRI dynamics is strongly mediated by k_{in}^w.

B. Correlations between topological node properties and rs-fMRI dynamics

Having demonstrated a strong relationship between the structural connectivity properties of a brain region and its rs-fMRI dynamics mediated most strongly by weighted in-degree, k_{in}^w, we next characterize the types of rs-fMRI time-series properties that drive the effect, focusing in on this key topological measure, k_{in}^w.

From inspecting the 3 003 rs-fMRI time-series properties that were significantly correlated with weighted in-degree, k_{in}^w ($|\rho| \geq 0.32$,$p_{\text{corrected}} < 0.05$), we found that they span a broad range time-series analysis methods, including measures of distribution spread and outliers, temporal entropies, autocorrelations, power spectral features, stationarity measures, fits to time-series models, wavelet measures, and methods from fluctutation analysis. To understand which of these diverse types of time-series features most strongly drive the relationship between k_{in}^w and rs-fMRI dynamics, we focused in on the 80 time-series features with the strongest correlations to k_{in}^w across the brain ($|\rho| \geq 0.55$), shown as a pairwise correlation matrix in Fig. 4. For all pairs of these top 80 time-series features, Fig. 4 shows their Spearman correlation across all 184 brain regions, with hierarchical linkage clustering (on distance metric $1 - |\rho|$) used to reorder the features for visualization. The figure reveals two main clusters of time-series properties, which we labeled as 'A' and 'B'. We selected the top 80 features as a manageable set to characterize in detail here, but note that increasing this number beyond 80 does not reveal any new structure until ≈ 1000 features are included, at which point the correlations between the features and k_{in}^w are much weaker, $\rho < 0.45$.

The first cluster of features, labeled 'A' in Fig. 4, are highly inter-correlated, and measure the spread of the rs-fMRI signal, including the inter-quartile range and mean absolute deviation. The weighted in-degree, k_{in}^w, is negatively correlated with these measures of BOLD signal spread, e.g., $\rho = -0.62$ with standard deviation. The second cluster, labeled 'B' in Fig. 4, contains features that measure correlation timescales in the fMRI signal, including the power in specific spectral frequency bands and the goodness of fit of sinusoidal and autoregressive models to the time series. The weighted in-degree, k_{in}^w, increases with the timescale of the fMRI signal (e.g., k_{in}^w is negatively correlated with the relative high-frequency power, $f \geq 0.375$ Hz: $\rho = -0.58$). Thus, using a highly comparative data-driven approach to univariate time-series characterization[38,39,52], we determine that k_{in}^w is the most informative network property for understanding regional

rs-fMRI dynamics, and that the time-series properties of the rs-fMRI dynamics that mostly strongly correlate with k_{in}^{w} are capturing two distinct types of signal properties: (i) spread of the BOLD signal (e.g., standard deviation), which decreases with increasing k_{in}^{w}, and (ii) power in different frequency bands of the BOLD signal, with reduced power for $f \geq 0.375\,\text{Hz}$ in brain regions with high k_{in}^{w}.

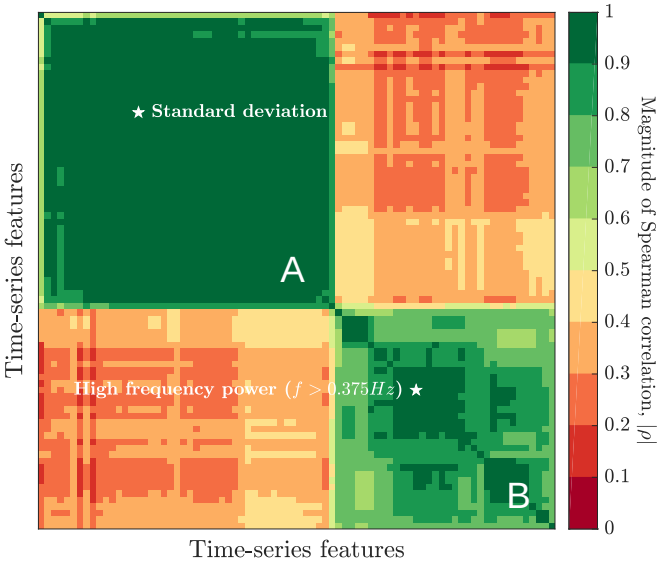

FIG. 4. **Features of the rs-fMRI signal that correlate most strongly with weighted in-degree across the brain form two clusters, related to the spread and correlation timescales in the BOLD dynamics.** Correlations between the 80 time-series features that correlated most strongly with weighted in-degree, k_{in}^{w}, are shown as an 80×80 pairwise correlation matrix using color. Feature-feature Spearman correlations are measured across 184 brain regions, and features have been reordered using hierarchical clustering (with an absolute correlation-based distance metric, $1 - |\rho|$), to place pairs of correlated features close to each other. These 80 time-series features fall into two clear clusters, labeled 'A': measures related to the spread of the BOLD signal (e.g., standard deviation), and 'B': measures related to correlation timescales in the signal (e.g., power in spectral frequency bands). Note that, this figure is reproduced larger in Fig. S3, where the names for all 80 features, and their correlations to k_{in}^{w} could be labeled. Two key features discussed in the text, standard deviation and high frequency power, are annotated with white stars.

We first focus on the negative correlation found between k_{in}^{w} and the spread of the rs-fMRI signal. The time-series feature with the highest Spearman correlation, $|\rho|$, to k_{in}^{w} across all 6 930 time-series features, is `MD_rawHRVmeas_SD1` ($\rho = -0.68$), which is a spread-dependent feature that lies in group 'A' of Fig. 4. This time-series feature is popular in the heart-rate variability literature, and is proportional to the standard deviation of the successive differences of the time series[54]. As shown in Fig. 4, features in group 'A' are highly intercorrelated, and this cluster also contains a simpler and more intuitive feature: the standard deviation of the time series, `standard_deviation` (annotated with a star in Fig. 4). The standard deviation exhibits a correlation to k_{in}^{w} of $\rho = -0.62$. Due to its ease of interpretation, we investigate the standard deviation of the BOLD signal in more detail as an intuitive representative of cluster 'A', shown as a scatterplot with k_{in}^{w} in Fig. 5(a). In this plot, each brain region is colored according to the Allen Reference Atlas[28,41], with colors broadly representing anatomical divisions of the mouse brain (as in Fig. 1). The plot reveals a strong negative relationship between weighted in-degree, k_{in}^{w}, and the standard deviation of the BOLD signal across the brain. The mix of colors in Fig. 5(a) reflects the fact that the negative relationship holds relatively consistently across anatomical brain divisions. For three specific brain regions annotated in Fig. 5(a): the subparafascicular area (SPA) of the thalamus ($k_{\text{in}}^{w} = 0.55$), the medial orbital area (ORBm) of the isocortex ($k_{\text{in}}^{w} = 4.39$), and the external nucleus of the inferior colliculus (ICe) of the midbrain ($k_{\text{in}}^{w} = 10.56$), we plotted the distribution of BOLD signal values as a smoothed density plot, shown in Fig. 5(b). The figure shows a clear decrease in the spread of the BOLD signal in brain regions with higher weighted in-degree, k_{in}^{w}.

The second group of time-series features, labeled 'B' in Fig. 4, consists of time-series features measuring different aspects of correlation timescales in the regional BOLD time series, including fitting oscillation models to the data, and extracting features from the power spectrum. The feature in this group with the strongest Spearman correlation to k_{in}^{w} is `SP_Summaries_pgram_hamm_linfitloglog_all_sigma` ($\rho = 0.60$), which computes the goodness of a linear fit to the log-log power spectrum of the BOLD signal (estimated as a periodogram using a Hamming window). This tells us that the log-log power spectrum of the BOLD signal is more linear in brain regions with higher k_{in}^{w}, a result with an intruiging connection to the relationship between brain network connectivity and scale-free brain dynamics[21,25]. However, we focus here on the more intuitive feature, `SP_Summaries_welch_rect_logarea_4_4`, labeled as a star in cluster 'B' of Fig. 4. This feature estimates the power spectral density of the BOLD signal using Welch's method[55], and then calculates the logarithm of the proportion of the power in the top quarter of frequencies (i.e., $f \geq 0.375\,\text{Hz}$), which we thus refer to as a measure of 'relative high frequency power' (where 'high' is the range from 0.375 Hz up to the sampling rate, 0.5 Hz). This feature displays a negative correlation with k_{in}^{w} ($\rho = -0.58$) across the brain, shown as a scatter in Fig. 5(c). That is, brain regions with increased k_{in}^{w} have decreased relative power in $f \geq 0.375\,\text{Hz}$ content in their rs-fMRI dynamics, or, equivalently, brain regions with increased k_{in}^{w} have greater relative power in $f < 0.375\,\text{Hz}$. This corresponds to brain regions with an overall increase in incoming connectivity weights exhibiting slower dynamics. Compared to standard deviation, shown in Fig. 5(a), the negative trend in relative high frequency power is dominated by a strong reduction in high

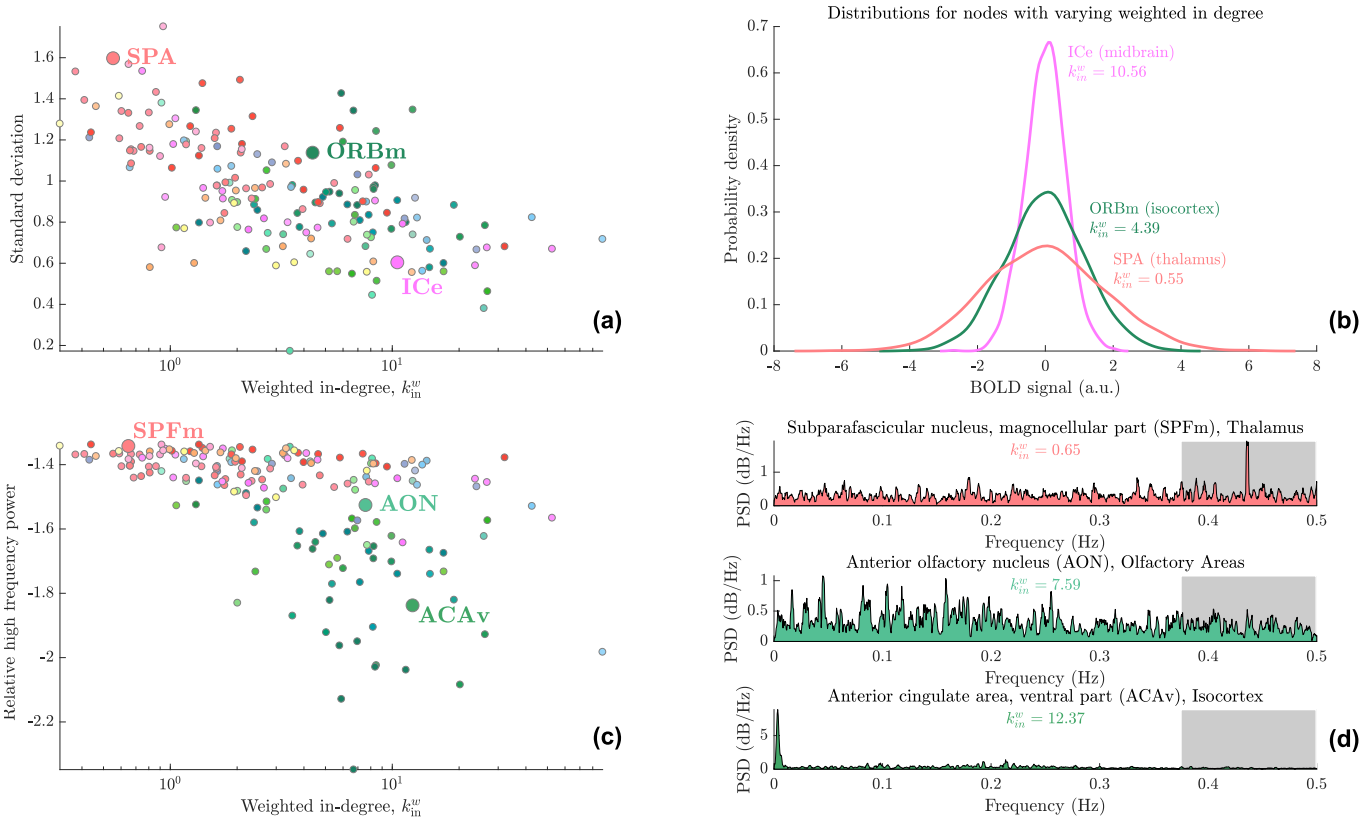

FIG. 5. **Weighted in-degree is negatively correlated with regional BOLD signal variability and relative high-frequency power.** Scatter plots of a brain region's weighted in-degree are shown against: **(a)** standard deviation of the rs-fMRI signal **(c)** relative power of the rs-fMRI signal in frequencies $f \geq 0.375\,\mathrm{Hz}$. Brain regions are colored uniquely, corresponding to anatomical divisions (cf. Fig. 1). For three selected brain regions (ICe = Inferior colliculus, external nucleus, ORBm = Orbital area, medial part, SPA = Subparafascicular area), highlighted and labeled in (a), we plot a kernel-smoothed distribution of their resting state BOLD time series in **(b)**, demonstrating a decrease in standard deviation for regions with a larger k^w_{in}. Similarly, for three labelled brain regions in (c), we show power spectral density estimates of their rs-fMRI signals using Welch's method (smoothed for visualisation) in **(d)**. The relative high frequency power measured in **(c)** corresponds to the logarithm of the proportion of the power in the top quarter of frequencies (shaded gray) of the power spectral density estimate, as calculated using Welch's method[55]. This corresponds to the frequency range $f \geq 0.375\,\mathrm{Hz}$, and is higher for regions with increased k^w_{in}.

frequency rs-fMRI dynamics in the cerebral cortex relative to the brainstem and cerebellum. To demonstrate the relationship in more detail, we plotted power spectral density estimates for three selected brain regions in Fig. 5(d): the magnocellular part of the subparafascicular nucleus (SPFm) in the thalamus ($k^w_{\mathrm{in}} = 0.65$), the anterior olfactory nucleus (AON) in the olfactory areas ($k^w_{\mathrm{in}} = 7.59$), and the ventral part of the anterior cingulate area (ACAv) in the isocortex ($k^w_{\mathrm{in}} = 12.37$), as annotated in Fig. 5(c). Frequencies exceeding $f = 0.375\,\mathrm{Hz}$ are shaded in Fig. 5(d), indicating the decrease in high frequency power in regions with greater total incoming structural connection weights.

As noted above, some dynamical properties of the rs-fMRI signal differ across anatomical divisions (as is evident by the visual disinction of particularly the isocortex and hippocampus in Fig. 1, lower right), and may thus result from broad anatomical differences, or non-specific spatial gradients in dynamics, rather than reflecting specific properties of network connectivity. To probe the contribution of space in contributing to variations in weighted in-degree, k^w_{in}, and the two types of features shown in Fig. 4, BOLD standard deviation and relative high frequency power, we mapped their variation across all brain regions in Fig. 6. The three-dimensional rendering for weighted in-degree, k^w_{in} in Fig. 6(a), clearly shows a specific, non-uniform distribution across the brain, with the highest values in the caudate-putamen (CPu), a region that integrates a large number of cortical and midbrain neural inputs, followed by the superior colliculus (SC), a subcortical area that integrates visual and sensory information, and the piriform cortex (Pir), which mediates olfactory processing. A similar spatial distribution is reflected in the variation of rs-fMRI standard deviation across the brain [Fig. 6(b), note inversion of color scale], which also exhibits a specific spatial patterning across brain regions. The relative high-frequency power is low in motor and somatosensory cortical regions,

in the caudoputamen and in the hippocampus, and high in the thalamus and midbrain.

To ensure that our results are not driven by broad anatomical variations or non-specific spatial gradients in BOLD dynamics (or connectivity properties) across the brain, we repeated our analysis using the 38 brain regions in the more homogeneous and spatially constrainted isocortex of the mouse brain. For this analysis we calculated the weighted in-degree, k^w_{in}, of each node of the cortical connectome, considering only cortico-cortical connectivity rather than the whole right hemisphere. Once again, significant negative correlations were observed between k^w_{in} and the standard deviation ($\rho = -0.38$, $p = 0.02$), and high frequency power ($\rho = -0.44$, $p = 0.006$). These correlations are weaker than those seen across the whole right hemisphere, indicating that to broad spatial variations may contribute in part to the relationship between k_{in} and rs-fMRI dynamics. However, our ability to reproduce the whole-brain result in the cortical connectome demonstrates that the intrinstic rs-fMRI dynamics of a brain region are closely related to its extrinstic axonal connectivity.

Above, we focused on characterising the time-series features that strongly correlate with k^w_{in}. However, as described in Sec. III A, many other network properties showed significant correlations to rs-fMRI across the brain, most notably, weighted degree, k^w, and weighted clustering coefficients, $C^{\rightarrow,w}$ and C^w. We demonstrated that, k^w, $C^{\rightarrow,w}$ and C^w did not capture unique information about rs-fMRI dynamics, with correlations to rs-fMRI properties mediated by k^w_{in}. Thus they should be expected to correlate with similar time-series properties as k^w_{in}. Indeed, we found that the rs-fMRI time-series features that were significantly correlated to k^w, $C^{\rightarrow,w}$ and C^w, were almost complete subsets of the 3 003 that displayed significant correlations with k^w_{in} (sharing over 96% of the same features). Thus, correlations between k^w, C^w, and $C^{\rightarrow,w}$ and rs-fMRI time-series properties, are weaker than corresponding correlations for k^w_{in}, and involve the same types of dynamical properties, supporting the view of k^w_{in} as the structural connectivity property mediating the relationship to regional dynamics.

Here we analyzed only the ipsilateral connectivity in the complete connectome available in the right hemisphere of the mouse brain. We note, however, that inclusion of contralateral projections, under the assumption of hemispheric symmetry (see Methods), yielded qualitatively similar results to those presented here. In particular, k^w_{in} remained the topological property with the strongest relationship to rs-fMRI dynamics, and exhibited similar correlations with standard deviation ($\rho = -0.60$) and high frequency power ($\rho = -0.53$).

C. Individual analysis

The results above involved characterizing the rs-fMRI dynamics of each brain region by averaging time-series features across all 18 individual mice. In this section, we investigate whether the results reported above between topological nodal measures and rs-fMRI dynamics, also hold on an individual level.

The key structural connectivity property, weighted in-degree, k^w_{in}, showed a group-level correlation with the standard deviation of BOLD of $\rho = -0.62$. The distribution of correlations across all eighteen individual mice is shown as a histogram in Fig. 7. The Spearman correlation, ρ, between k^w_{in} and rs-fMRI standard deviation was significant and highly consistent for each individual mouse ($p_{\text{corrected}} < 0.05$, correcting for the comparisons across the eighteen mice), with individual correlations remaining high and relatively consistent, ranging from $\rho = -0.68$ to $\rho = -0.51$. The relative high frequency power ($f \geq 0.375\,\text{Hz}$) feature characterized above also exhibited consistent and significant correlations for all eighteen individual mice. Indeed, 72 of the 80 features shown in Fig. S3, exhibited correlations that remain significant on an individual-level for all 18 mice.

Our results indicate that the relationships shown above using group-level dynamical summaries of the rs-fMRI data, are not a consequence of averaging over individuals, but hold on an individual level.

IV. DISCUSSION

In this work we used a weighted, directed mesoscale structural connectome and high quality rs-fMRI measurements across 184 anatomical brain regions to demonstrate a robust relationship between a brain region's topological role in the structural connectome and its resting state dynamics in the mouse. Rather than analysing pairwise structure-function relationships, our results provide the first characterization of a potential role of structural connectivity in shaping the dynamics of individual brain regions. We show that weighted and directed information is required to optimally uncover the regional structure-function relationship, and that the weight of incoming projections to a region is the primary correlate for regional BOLD dynamics, particularly with respect to its variability and correlation timescales. As well as providing new insights into the role of structural connectivity in the brain, our empirical results may provide a new means of constraining the models we use to simulate and understand brain dynamics.

The nodal network properties analyzed here can be divided into measures of immediate connectivity (degree, k), neighborhood connectivity (clustering coefficient, C), and global connectivity (betweenness centrality, b). The strongest correlations between nodal connectivity and rs-fMRI dynamics were found for degree-based measures of immediate connectivity, with the strongest correlation found for weighted in-degree, k^w_{in}, the weighted sum of inputs from other brain regions. The weighted in-degree was significantly correlated to 3 003 time-series rs-fMRI time-series properties (from a set of 6 930, $p_{\text{corrected}} <$

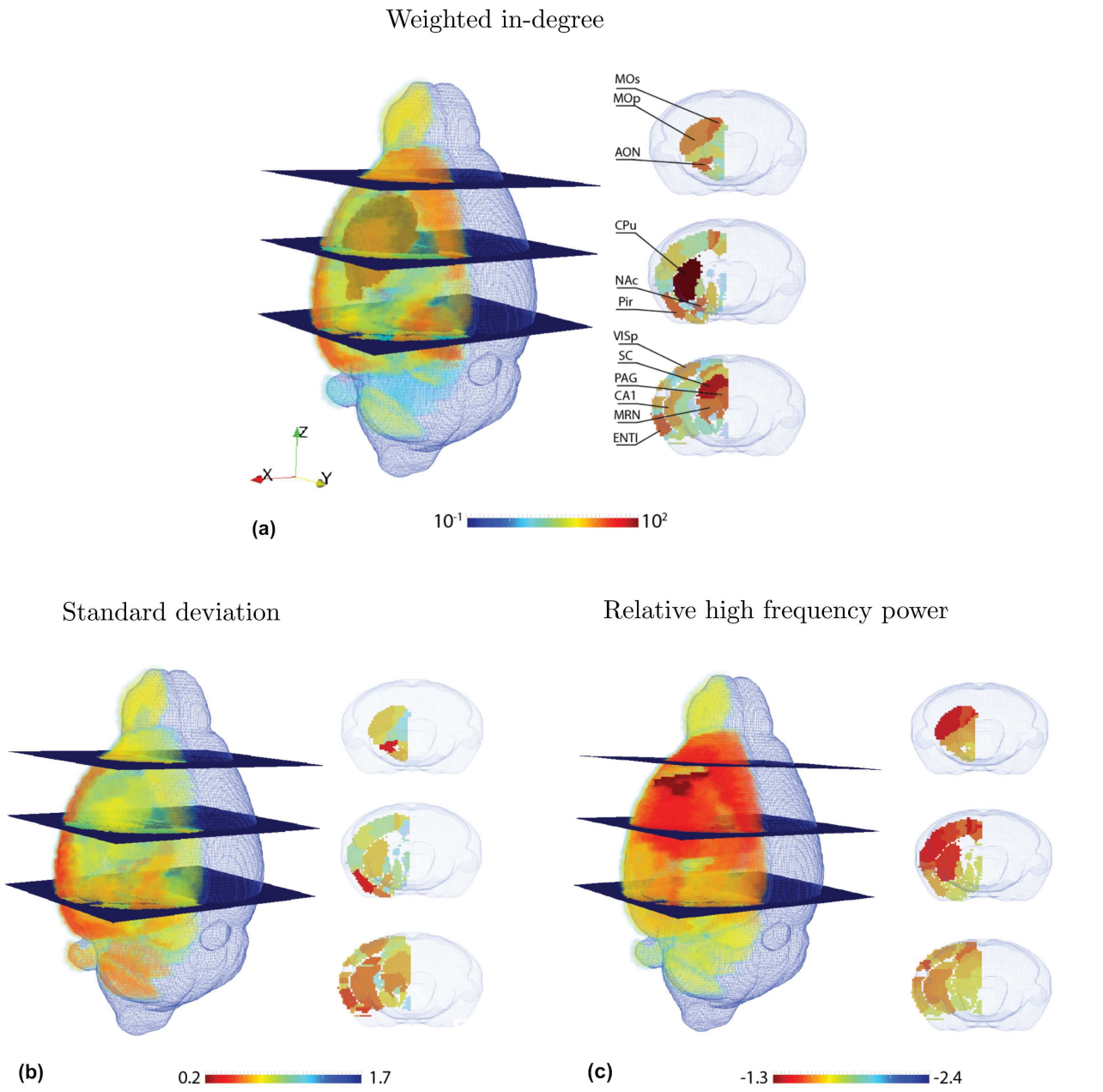

FIG. 6. A three-dimensional rendering of the spatial mapping of 184 regions across the right hemisphere of the mouse brain for: **(a)** the topological quantity, weighted in-degree, $\log_{10} k^w_{\text{in}}$, **(b)** standard deviation of the BOLD signal (note inverted color scale), and **(c)** relative high frequency BOLD power ($f \geq 0.375\,\text{Hz}$, note inverted color scale). Highlighted in the 2D slices in **(a)** are the twelve regions with the highest weighted-in degree. Labelled regions are: MOp, MOs = primary and secondary motor cortex; AON = anterior olfactory nucleus; CPu = Caudoputamen; NAc = nucleus accumbens; Pir = piriform cortex; VISp = primary visual area; SC = superior colliculus; PAG = periaqueductal gray; CA1 = cornus ammonis 1; MRN = midbrain reticular nucleus; ENTI = entorhinal area.

0.05), with Spearman correlations reaching up to $|\rho| = 0.68$. Given the diversity of regions across the whole brain analyzed here, including regions that differ in terms of their functional specialization, gene expression, and cellular and microcircuit properties[28,29], all of which may affect regional dynamics (cf.[14,59]), this level of correlation with just the incoming mesoscale connectivity to a brain region, k^w_{in}, is remarkable. Other properties, like the global measure of betweenness centrality, b, showed minimal correlations to dynamics (potentially related to

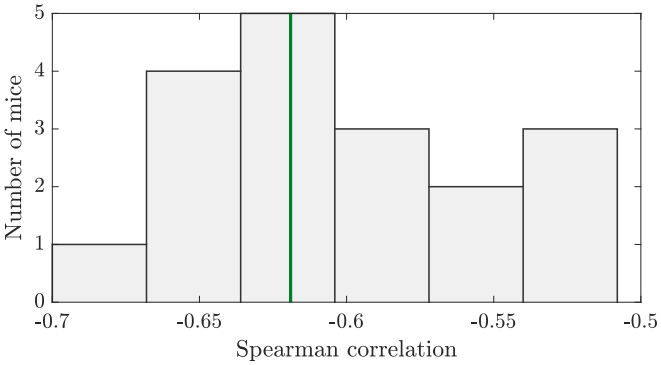

FIG. 7. **Weighted in-degree shows a robust and significant negative correlation to the standard deviation of the rs-fMRI signal for all individual mice**. Here we plot the distribution, across eighteen individual mice, of the Spearman correlation between weighted in-degree and rs-fMRI standard deviation over all 184 brain regions. The green vertical line indicates the correlation value when the standard deviation in each brain region is taken as the average across all individuals.

the fact that information transmission across brain networks may more closely follow an unguided, diffusion-like process rather than shortest paths[5,23,26]). Structural network properties other than $k^w_{\rm in}$ that showed strong and significant correlations to rs-fMRI dynamics—k^w, C^w, and $C^{\rightarrow,w}$—were driven by their correlation to $k^w_{\rm in}$ across the brain; these measures were related to the same types of time-series properties as $k^w_{\rm in}$ and showed minimal correlations to rs-fMRI dynamics when $k^w_{\rm in}$ was controlled for. Thus, although the clustering coefficient measures distinct information to weighted in-degree, $k^w_{\rm in}$ (e.g., broadly distinguishing different local connectivity motifs that have been proposed to have distinctive functional roles and dynamics[56–58]), our results indicate that it does not provides unique information about rs-fMRI dynamics. Taken together, our results distinguish $k^w_{\rm in}$ as the key driver of the regional structure-function relationship, and indicate that incoming influences from other areas are closely tied to a region's spontaneous dynamics. Our findings may also reflect the haemodynamic measure of neuronal activity provided by the BOLD signal. The strongest neurophysiological correlate of the BOLD signal is the local field potential, which is more strongly driven by local synaptic integration of incoming signals rather than spiking output[60,61]. Whether the close association between incoming connectivity and dynamics reported here for mesoscopic brain regions would also hold using single unit recordings of individual neurons remains an open question.

Rather than hand-picking particular time-series features to investigate for rs-fMRI, our highly comparative approach compared over 6 930 time-series features of fMRI in a purely data-driven way, including time-series model fitting and prediction, entropies, distributional measures, and other types of linear and nonlinear correlation features[38,39,52]. Of the 3 003 properties of regional rs-fMRI dynamics that were significantly correlated to weighted in-degree, $k^w_{\rm in}$, those with the strongest relationship formed two clusters: one containing measures of the spread of the BOLD signal, and the other containing measures of correlation timescales, including power in spectral frequency bands, sinusoidal model fits, and the linearity of the log-log power spectrum. Selecting the simplest measures from each cluster to aid interpretation, we determined that $k^w_{\rm in}$ was most distinctively characterized by BOLD dynamics with reduced variance and reduced relative high frequency power ($0.375\,{\rm Hz} \leq f \leq 0.5\,{\rm Hz}$ or, equivalently, increased power in low-mid frequencies, $f < 0.375$). These effects found at the group level for the whole brain were highly robust, being reproduced for all eighteen individual mice, and when just analyzing the reduced cortical network. To our knowledge, this is the first report of a relationship between brain connectivity and the standard deviation of BOLD dynamics. The negative relationship between $k^w_{\rm in}$ and fMRI signal variance was highly significant, and driven by variation within and across broad anatomical divisions of the mouse brain, including the brain stem, cerebellum, and cerebrum. The finding goes against the intuitive view that stronger inputs increase the variance of the dynamics in a brain region, and may be key to better constraining our models of brain dynamics in the future. The highly comparative approach used here also selected time-series properties related to correlation timescales as being highly correlated with $k^w_{\rm in}$, with brain regions with stronger inputs exhibiting slower dynamics (greater relative power in $f < 0.375\,{\rm Hz}$). This is consistent with a connectivity-mediated hierarchy of timescales in the brain[13,14]. In Gollo et al.[13], nonlinear neural mass models were coupled via an unweighted, directed macaque structural connectome, producing an emergent dynamical hierarchy in which highly connected hub regions exhibited greater temporal persistence in their dynamics, largely due to their high (unweighted) in-degree. In Chaudhuri et al.[14], an interplay of intrinsic variation in timescales across cortical brain regions, inter-areal connectivity, and input to the brain determined the dynamical timescale of a brain region (estimated as the decay time constant of the autocorrelation function). Our work thus provides new insights into the role of the connectome in contributing to a variation of dynamical timescales across the brain.

Our tract-tracing derived mouse connectivity data allowed us to investigate the role of edge weights and directionality in contributing to the relationship between the structural connectome and fMRI dynamics. In particular, we compared measures computed from the original weighted, directed connectome[40], as well as unweighted and undirected approximations to it. Although unweighted brain networks are more intuitive and amenable to the application of graph theoretic techniques that have been popular in connectomic research, one might expect that incorporating meaningful estimates of edge weights

into brain network analysis is important, as they vary over several orders of magnitude (see Fig. S1). Indeed, given recent estimates of cortical connection densities from high-quality tract-tracing data exceeding 60% for macaque cortex[62,63] and 70% for mouse cortex[64], binary representations of such dense connectomes constitute coarse approximations of true brain connectivity. Here we demonstrate that network properties derived from unweighted connectomes show negligible correlations to properties of rs-fMRI, supporting the importance of connectome edge weights in capturing the relationship between connectivity and dynamics in the mouse brain. We note that the estimation of edge weights from tract-tracing based experiments is non-trivial, and while here we used normalized connection densities derived from the regression model of Oh et al.[40], alternative estimation methods[64,65] and datasets[66] exist. Given that human connectomes are commonly estimated by tractography using diffusion weighted imaging (DWI), which is noisy and cannot determine the direction of a pathway, it is important to note that k^w is significantly correlated with similar types of features of rs-fMRI dynamics as k^w_{in}. This suggests that, if similar connectivity-dynamics relationships hold in human as in mouse, then the undirected connectome estimated using DTI should constitue a useful approximation to the connectome, despite limiting our ability to capture the strongest structure-function relationships mediated by k^w_{in}. In addition to edge weights, we found that directed edge information was critical for distinguishing the weighted out-degree of a node, k^w_{out}, which is relatively uninformative of rs-fMRI dynamics, from the highly informative weighted in-degree, k^w_{in}. Indeed, the importance of taking edge weight and directionality into account in relating structure to function suggests that the coupling of tract-tracing based connectomes with measurements of dynamics in model animals will be crucial to understanding how brain dynamics are constrained by extrinsic axonal connectivity, and will be key in constraining computational models of brain dynamics in future work.

The mouse represents an extremely attractive model system to study the structure-function relationship, while minimizing the influence of environmental and genetic heterogeneity. Our findings relied on long (38 min), high-quality rs-fMRI measurements of BOLD dynamics across the whole mouse brain, which were compared to the a tract-tracing based structural connectome for the first time in this work. The use of awake mice in rs-fMRI protocols is impracticable for long scan times (notwithstanding the use of invasive methods for head fixation[68]), making light anesthesia the *de facto* option[69]. Due to the technical and methodological challenges in obtaining such long functional scans in an anesthetized regime, one must take care that the physiology of the animals remains stable over time. Several parameters were considered in this study to achieve this goal; first, we used mechanical ventilation to maintain the same tidal volume and blood oxygenation throughout the experiment. To keep a low but steady level of anesthesia, we combined a continue infusion of medetomedine i/v with a very low dose of isoflurane (0.5%), optimized from our previous studies[42,67]; this allowed us to overcome the issues related to medetomidine depletion and isoflurane accumulation over time. As evidenced by our results, which showed high consistency across all eighteen mice, this protocol allows for superior data reproducibility due to a drastic reduction in motion, stable physiology such as animal temperature and stress levels, and a regular breathing cycle.

V. CONCLUSION

In this work, we provide the first demonstration of a robust relationship between the connectivity properties of a brain region and resting state BOLD dynamics. The strongest relationships are for the weighted in-degree of a brain region, which is negatively correlated to the standard deviation and relative high frequency power ($f \geq 0.375\,\text{Hz}$) of its rs-fMRI dynamics. Our results are consistent with physiological data indicating that BOLD signal modulations reflect the integration of incoming signals, and support preliminary predictions of computational models suggesting a role for connectivity in mediating differences in the intrinsic dynamical timescales of distinct regions across the brain. Our results also highlight the importance of directed and weighted information for understanding brain communication across the connectome.

ACKNOWLEDGMENTS

We would like to thank L. Gollo for providing valuable advice and feedback on the manuscript. We would like also to acknowledge G. Ielacqua and M. Markicevic for their precious help during the MRI experiments. B.D.F. is supported by a NHMRC Early Career Fellowship (1089718). A.F. is supported by an ARC Future Fellowship (FT130100589) and NHMRC Project Grants (1066779 and 1050504). The authors declare no competing financial interests.

[1] O. Sporns. The human connectome: a complex network. *Ann. N.Y. Acad. Sci.* **1224**, 109 (2011).

[2] G. Deco, P. A. Robinson, V. K. Jirsa, M. J. Breakspear, and K. J. Friston. The Dynamic Brain: From Spiking Neurons to Neural Masses and Cortical Fields. *PLoS Comp. Biol.* **4**, e1000092 (2008).

[3] C. J. Honey, O. Sporns, L. Cammoun, et al. Predicting human resting-state functional connectivity from structural connectivity. *Proc. Natl. Acad. Sci. USA* **106**, 2035 (2009).

[4] P. Skudlarski, K. Jagannathan, and V. D. Calhoun. Measuring brain connectivity: diffusion tensor imaging validates resting state temporal correlations. *NeuroImage* (2008).

[5] J. Goñi, M. P. van den Heuvel, A. Avena-Koenigsberger, et al. Resting-brain functional connectivity predicted by analytic measures of network communication. *Proc. Natl. Acad. Sci. USA* **111**, 833 (2014).

[6]A. Zalesky and A. Fornito. A DTI-Derived Measure of Cortico-Cortical Connectivity. *IEEE Trans. Med. Imaging* **28**, 1023 (2009).

[7]H. Finger, M. Bönstrup, B. Cheng, et al. Modeling of Large-Scale Functional Brain Networks Based on Structural Connectivity from DTI: Comparison with EEG Derived Phase Coupling Networks and Evaluation of Alternative Methods along the Modeling Path. *PLoS Comp. Biol.* **12**, e1005025 (2016).

[8]C. J. Honey, J.-P. Thivierge, and O. Sporns. Can structure predict function in the human brain? *NeuroImage* **52**, 766 (2010).

[9]C. J. Honey, M. Breakspear, R. Kötter, and O. Sporns. Network structure of cerebral cortex shapes functional connectivity on multiple time scales. *Proc. Natl. Acad. Sci. USA* **104**, 10240 (2007).

[10]P. Hagmann, G. Deco, A. Ponce-Alvarez, et al. Resting-State Functional Connectivity Emerges from Structurally and Dynamically Shaped Slow Linear Fluctuations. *J. Neurosci.* **33**, 11239 (2013).

[11]B. Mišić, R. F. Betzel, M. A. de Reus, et al. Network-Level Structure-Function Relationships in Human Neocortex. *Cereb. Cortex* **26**, 3285 (2016).

[12]M. J. Breakspear, J. R. Terry, and K. J. Friston. Modulation of excitatory synaptic coupling facilitates synchronization and complex dynamics in a biophysical model of neuronal dynamics. *Network: Comput. Neural Syst.* **14**, 703 (2003).

[13]L. L. Gollo, A. Zalesky, R. M. Hutchison, M. P. van den Heuvel, and M. J. Breakspear. Dwelling quietly in the rich club: brain network determinants of slow cortical fluctuations. *Phil. Trans. Roy. Soc. B* **370**, 20140165 (2015).

[14]R. Chaudhuri, K. Knoblauch, M.-A. Gariel, H. Kennedy, and X.-J. Wang. A Large-Scale Circuit Mechanism for Hierarchical Dynamical Processing in the Primate Cortex. *Neuron* **88**, 419 (2015).

[15]R. F. Galán. On How Network Architecture Determines the Dominant Patterns of Spontaneous Neural Activity. *PLoS ONE* **3**, e2148 (2008).

[16]F. Abdelnour, H. U. Voss, and A. Raj. Network diffusion accurately models the relationship between structural and functional brain connectivity networks. *NeuroImage* **90**, 335 (2014).

[17]A. Raj, A. Kuceyeski, and M. Weiner. A network diffusion model of disease progression in dementia. *Neuron* p. 1204 (2012).

[18]M. J. Breakspear, S. Heitmann, and A. Daffertshofer. Generative models of cortical oscillations: neurobiological implications of the Kuramoto model. *Front. Hum. Neurosci.* (2010).

[19]J. Cabral, E. Hugues, and O. Sporns. Role of local network oscillations in resting-state functional connectivity. *NeuroImage* **57**, 130 (2011).

[20]L. Cocchi, M. V. Sale, L. L. Gollo, et al. A hierarchy of timescales explains distinct effects of local inhibition of primary visual cortex and frontal eye fields. *eLife Sciences* **5**, e15252 (2016).

[21]G. Deco and V. K. Jirsa. Ongoing Cortical Activity at Rest: Criticality, Multistability, and Ghost Attractors. *J. Neurosci.* **32**, 3366 (2012).

[22]G. Deco, A. R. McIntosh, K. Shen, et al. Identification of optimal structural connectivity using functional connectivity and neural modeling. *J. Neurosci.* **34**, 7910 (2014).

[23]B. Mišić, R. F. Betzel, A. Nematzadeh, et al. Cooperative and Competitive Spreading Dynamics on the Human Connectome. *Neuron* **86**, 1518 (2015).

[24]G. Deco, V. K. Jirsa, and A. R. McIntosh. Emerging concepts for the dynamical organization of resting-state activity in the brain. *Nat. Rev. Neurosci.* **12**, 43 (2011).

[25]A. Haimovici, E. Tagliazucchi, P. Balenzuela, and D. R. Chialvo. Brain Organization into Resting State Networks Emerges at Criticality on a Model of the Human Connectome. *Phys. Rev. Lett.* **110**, 178101 (2013).

[26]J. Goñi, A. Avena-Koenigsberger, N. V. de Mendizabal, et al. Exploring the Morphospace of Communication Efficiency in Complex Networks. *PLoS ONE* **8** (2013).

[27]B. Mišić, O. Sporns, and A. R. McIntosh. Communication Efficiency and Congestion of Signal Traffic in Large-Scale Brain Networks. *PLoS Comp. Biol.* **10**, e1003427 (2014).

[28]E. Lein, M. J. Hawrylycz, N. Ao, et al. Genome-wide atlas of gene expression in the adult mouse brain. *Nature* **445**, 168 (2007).

[29]L. Madisen, T. A. Zwingman, S. M. Sunkin, et al. A robust and high-throughput Cre reporting and characterization system for the whole mouse brain. *Nat. Neurosci.* **13**, 133 (2010).

[30]R. E. Passingham, K. E. Stephan, and R. Kötter. The anatomical basis of functional localization in the cortex. *Nat. Rev. Neurosci.* **3**, 606 (2002).

[31]A. Keitel and J. Gross. Individual Human Brain Areas Can Be Identified from Their Characteristic Spectral Activation Fingerprints. *PLoS Biol.* **14**, e1002498 (2016).

[32]D. J. Felleman and D. C. Van Essen. Distributed Hierarchical Processing in the Primate Cerebral Cortex. *Cereb. Cortex* **1**, 1 (1991).

[33]S. J. Kiebel, J. Daunizeau, and K. J. Friston. A Hierarchy of Time-Scales and the Brain. *PLoS Comp. Biol.* **4**, e1000209 (2008).

[34]C. J. Honey, T. Thesen, T. H. Donner, et al. Slow Cortical Dynamics and the Accumulation of Information over Long Timescales. *Neuron* **76**, 423 (2012).

[35]G. J. Stephens, C. J. Honey, and U. Hasson. A place for time: the spatiotemporal structure of neural dynamics during natural audition. *J. Neurophysiol.* **110**, 2019 (2013).

[36]J. D. Murray, A. Bernacchia, D. J. Freedman, et al. A hierarchy of intrinsic timescales across primate cortex. *Nat. Neurosci.* **17**, 1661 (2014).

[37]J. Chen, U. Hasson, and C. J. Honey. Processing Timescales as an Organizing Principle for Primate Cortex. *Neuron* **88**, 244 (2015).

[38]B. D. Fulcher, M. A. Little, and N. S. Jones. Highly comparative time-series analysis: the empirical structure of time series and their methods. *J. Roy. Soc. Interface* **10**, 20130048 (2013).

[39]B. D. Fulcher and N. S. Jones. Automatic time-series phenotyping using massive feature extraction. *bioRxiv* p. 081463 (2016).

[40]S. W. Oh, J. A. Harris, L. Ng, et al. A mesoscale connectome of the mouse brain. *Nature* **508**, 207 (2014).

[41]H.-W. Dong. *The Allen reference atlas: A digital color brain atlas of the C57Bl/6J male mouse*. John Wiley & Sons Inc., Hoboken, NJ, US (2008).

[42]V. Zerbi, J. Grandjean, M. Rudin, and N. Wenderoth. Mapping the mouse brain with rs-fMRI: An optimized pipeline for functional network identification. *NeuroImage* **123**, 11 (2015).

[43]C. F. Beckmann and S. M. Smith. Probabilistic Independent Component Analysis for Functional Magnetic Resonance Imaging. *IEEE Trans. Med. Imaging* **23**, 137 (2004).

[44]M. Jenkinson, P. Bannister, M. Brady, and S. Smith. Improved Optimization for the Robust and Accurate Linear Registration and Motion Correction of Brain Images. *NeuroImage* **17**, 825 (2002).

[45]L. Griffanti, G. Salimi-Khorshidi, C. Beckmann, et al. ICA-based artefact removal and accelerated fMRI acquisition for improved resting state network imaging. *NeuroImage* **95**, 232 (2014).

[46]L. C. Freeman. A Set of Measures of Centrality Based on Betweenness (1977).

[47]D. J. Watts and S. H. Strogatz. Collective dynamics of 'small-world' networks. *Nature* **393**, 440 (1998).

[48]J.-P. Onnela, J. Saramäki, J. Kertész, and K. Kaski. Intensity and coherence of motifs in weighted complex networks. *Phys. Rev. E* **71**, 065103 (2005).

[49]G. Fagiolo. Clustering in complex directed networks. *Phys. Rev. E - Stat. Nonlinear, Soft Matter Phys.* **76** (2007).

[50]M. Rubinov and O. Sporns. Complex network measures of brain connectivity: Uses and interpretations. *NeuroImage* **52**, 1059 (2010).

[51]Z. Yu-Feng, H. Yong, Z. Chao-Zhe, et al. Altered baseline brain activity in children with ADHD revealed by resting-state functional MRI. *Brain Dev.* **29**, 83 (2007).

[52]B. D. Fulcher and N. S. Jones. Highly comparative feature-based time-series classification. *IEEE Trans. Knowl. Data Eng.* **26**, 3026 (2014).

[53]S. Holm. A Simple Sequentially Rejective Multiple Test Procedure. *Scand. J. Stat.* **6**, 65 (1979).

[54]M. Brennan, M. Palaniswami, and P. Kamen. Do existing measures of Poincare plot geometry reflect nonlinear features of heart rate variability? *IEEE Trans. Biomed. Eng.* **48**, 1342 (2001).

[55]P. Welch. The use of fast fourier transform for the estimation of power spectra: A method based on time averaging over short, modified periodograms. *IEEE Trans. Audio Electroacust.* **15**, 70 (1967).

[56]O. Sporns and R. Kötter. Motifs in Brain Networks. *PLoS Biol.* **2**, e369 (2004).

[57]L. L. Gollo, C. Mirasso, O. Sporns, and M. J. Breakspear. Mechanisms of Zero-Lag Synchronization in Cortical Motifs. *PLoS Comp. Biol.* **10**, e1003548 (2014).

[58]A. Azulay, E. Itskovits, and A. Zaslaver. The C . elegans Connectome Consists of Homogenous Circuits with Defined Functional Roles. *PLoS Comp. Biol.* **12**, e1005021 (2016).

[59]A. H. Marblestone, G. Wayne, and K. P. Kording. Toward an integration of deep learning and neuroscience. *Front. Comput. Neurosci.* **10**, 406 (2016).

[60]N. K. Logothetis, J. Pauls, M. Augath, T. Trinath, and A. Oeltermann. Neurophysiological investigation of the basis of the fMRI signal. *Nature* **412**, 150 (2001).

[61]M. Lauritzen and L. Gold. Brain function and neurophysiological correlates of signals used in functional neuroimaging. *J. Neurosci.* **23**, 3972 (2003).

[62]N. T. Markov, M. M. Ercsey-Ravasz, and A. Gomes. A weighted and directed interareal connectivity matrix for macaque cerebral cortex. *Cereb. Cortex* (2012).

[63]N. T. Markov, M. Ercsey-Ravasz, D. C. Van Essen, et al. Cortical High-Density Counterstream Architectures. *Science* **342**, 1238406 (2013).

[64]R. J. F. Ypma and E. Bullmore. Statistical Analysis of Tract-Tracing Experiments Demonstrates a Dense, Complex Cortical Network in the Mouse. *PLoS Comp. Biol.* **12**, e1005104 (2016).

[65]M. Rubinov, R. J. F. Ypma, C. Watson, and E. Bullmore. Wiring cost and topological participation of the mouse brain connectome. *Proc. Natl. Acad. Sci. USA* **112**, 10032 (2015).

[66]B. Zingg, H. Hintiryan, L. Gou, et al. Neural Networks of the Mouse Neocortex. *Cell* **156**, 1096 (2014).

[67]J. Grandjean, A. Schroeter, I. Batata, and M. Rudin. Optimization of anesthesia protocol for resting-state fMRI in mice based on differential effects of anesthetics on functional connectivity patterns. *Neuroimage* **102 Pt 2**, 838 (2014).

[68]K. Yoshida, Y. Mimura, R. Ishihara, et al. Physiological effects of a habituation procedure for functional MRI in awake mice using a cryogenic radiofrequency probe. *J. Neurosci. Methods* **274**, 38 (2016).

[69]E. Jonckers, R. Delgado y Palacios, D. Shah, et al. Different anesthesia regimes modulate the functional connectivity outcome in mice. *Magn. Reson. Med.* **72**, 1103 (2014).